Observer Designs for Experimental Non-Smooth and Discontinuous Systems

Apostolos Doris, Aleksandar Lj. Juloski, Nenad Mihajlović, W. P. M. H. (Maurice) Heemels, Nathan van de Wouw, and Henk Nijmeijer

***Abstract*—This brief presents the design and implementation of observer design strategies for experimental non-smooth continuous and discontinuous systems. First, a piece-wise linear observer is implemented for an experimental setup consisting of a harmonically excited flexible steel beam with a one-sided support which can be considered as a benchmark for a class of flexible mechanical systems with one-sided restoring characteristics. Second, an observer is developed for an experimental setup that describes a dynamic rotor system which is a benchmark for motion systems with friction and flexibility. In both cases, the implemented observers guarantee global asymptotic stability of the estimation error dynamic in theory. Simulation and experimental results are presented to demonstrate the performance of the observers in practice. These results support the use of (switched) observers to achieve state reconstruction for such non-smooth and discontinuous mechanical systems.**

***Index Terms*—Continuous piece-wise linear (PWL) systems, discontinuous systems, switching observer.**

I. Introduction

THE MOTIVATION for this work originates from the need to analyse and control the dynamics of complicated engineering constructions with non-smooth and discontinuous dynamics. An important class of engineering systems exhibiting non-smooth dynamics are mechanical systems comprising structural elements with piece-wise linear (PWL) restoring characteristics, such as tower cranes, suspension bridges [1], solar panels on satellites [2], or floating platforms for oil exploration [3]. Another relevant class of engineering systems consists of mechanical systems with discontinuities due to friction, such as industrial robots, drilling rigs [4], pick and place machines [5], turbine blade dampers [6], and many more. A common characteristic of all the mentioned applications is the non-smooth nature of their dynamics.

As the complete state of the aforementioned systems usually cannot be measured, it is convenient to have an accurate estimate of the complete system state in order to control these systems. Accurate estimates can be obtained using properly designed observers, given a model and measured input–output data of the system. Although in the linear and smooth setting observer design is well understood, in the nonlinear and non-smooth context the reconstruction of the state is far more difficult, in particular, if one faces the inherent difficulties of an experimental engineering environment (modeling errors, sensor noise, etc.). The overall objective of this work is the design and experimental validation of observers for certain classes of non-smooth and discontinuous systems in the field of applied mechanics and engineering.

In literature, various observer designs for non-smooth Lipschitzian systems are available. Sliding mode observers (see [7]) are designed for a class of non-smooth systems. These observers guarantee local asymptotic stability of the state estimation error. In [8], it was shown that in case of a nonlinear dynamical system with a scalar nonlinearity a Kalman filter can be used for state estimation. The drawback of this method is that the calculation of the observer gains relies on a trial-and-error technique. A more general approach for the state estimation of the aforementioned class of systems can be taken by using a switching Kalman filter (see [9]). Herein, different observer gains are used for different modes. An important drawback of both Kalman filter designs is that stability in general cannot be proven *a priori*. In [10] and [11], it is proven that the state estimation error of a model-based observer for a Lipschitzian system with slope-restricted possibly monotone multivariable nonlinearities, exponentially converges to zero. In [12], switched observers are considered for a class of bimodal PWL systems. The observer design strategy employed there provides sufficient conditions, under which global asymptotic stability of the state estimation error can be achieved if the system dynamics is continuous over the switching plane. In [13], a constructive observer design procedure for a class of non-smooth dynamical systems, namely systems of Lur'e type with a monotone multivalued mapping in the feedback path, is presented. Under certain passivity-related assumptions the observer asymptotically recovers the state of the observed system. The design in [13] is based on ideas in [14], in which monotone multivalued mappings were first introduced in the control community. It is a distinguishing feature of the observer structures in [10], [12], and [13] that the observers do not need knowledge about the active mode of the system, in contrast to those in [8] and [9]. A difference between [10] and [12], for the bimodal case, is that the observer design in [10] implies that the same observer gain is used for both modes, while in [12], different observer gains are used for every mode. A difference between [10], [12], and [13] is that the results of [10] are applicable to locally Lipschitzian systems while the results of [12] and [13] can also be applied to non-smooth, non-Lipschitzian systems.

The focus of this brief is on the design and implementation of: 1) a non-smooth PWL observer on a harmonically excited experimental PWL beam setup and 2) a discontinuous observer

Manuscript received January 4, 2007; revised November 6, 2007. Manuscript received in final form December 12, 2007. First published August 22, 2008; current version published October 22, 2008. Recommended by Associate Editor P. Mostarman. This work was supported in part by the European Projects SICONOS (IST2001-37172) and HYCON Network of Excellence (FP6-IST-511368).

A. Doris, N. van de Wouw, W. P. M. H. Heemels, and H. Nijmeijer are with the Department of Mechanical Engineering, Eindhoven University of Technology, 5600 MB Eindhoven, The Netherlands (e-mail: a.doris@tue.nl; n.v.d.wouw@tue.nl; m.heemels@tue.nl; h.nijmeijer@tue.nl).

A. Lj. Juloski is with Siemens AG, Erlangen 91052, Germany (e-mail: aleksandar.juloski@siemens.com).

N. Mihajlović is with Philips Research, Eindhoven 5656AE, The Netherlands (e-mail: nenad.mihajlovic@philips.com).

Digital Object Identifier 10.1109/TCST.2008.917236

based on [13] on an experimental dynamic rotor system with discontinuous friction. The PWL beam setup can be considered as a benchmark system for the implementation of observer and controller design strategies to complex engineering systems with PWL characteristics. More specifically, this system captures the basic dynamics of the aforementioned mechanical systems and reveals the fundamental practical problems that one faces when designing observers for such systems. Namely, the available measurements can hardly ever detect the moment of switching between the different dynamic regimes of such mechanical systems, since commonly the switching boundary for these systems is characterized by a combination of the components of the system state. Very often, it is very difficult and/or very expensive to use measurement devices to measure all of these state components in practice. The dynamic rotor system can be seen as a benchmark system for observer and controller design strategies for engineering systems with discontinuities due to friction. In such engineering systems the presence of friction induces a vibrational phenomenon (stick-slip limit cycles) that results in kinetic energy dissipation, noise, excessive wear of machine parts, and inferior positioning properties. Due to the fact that the examined system reproduces this kind of behavior it can be considered as benchmark for this type of systems.

For the description of the dynamics of the experimental setups, we use relatively simple low-order models, which, however, exhibit non-smooth or discontinuous characteristics. Such models are shown to be highly predictive for the experimental systems (see [4] and [15]) while exhibiting a limited model complexity. This motivates, first, the validity of non-smooth continuous and discontinuous modeling for engineering systems and, second, the need for the design of model-based observers for these types of non-smooth and discontinuous systems.

This brief is structured as follows. The observer design strategies that we will use are introduced in Section II. In Section III, a description of the PWL beam system is given and the observer design and implementation for this system are presented together with simulation and experimental results related to the observer performance. In Section IV, the experimental dynamic rotor system is presented, the observer design and implementation on this system are explained and simulation and experimental results are given. Discussions, conclusions, and directions for future work are given in Sections V and VI, respectively.

II. Observer Design for Non-Smooth and Discontinuous Systems

A. Observer Design for Bimodal PWL Systems

Consider a continuous-time bimodal PWL system of the following type:

$$\dot{x} = \begin{cases} A_1 x + Bu, & \text{if } H^T x \leq 0 \\ A_2 x + Bu, & \text{if } H^T x > 0 \end{cases} \tag{1}$$

with $y := Cx \in \mathbb{R}^p$, $x \in \mathbb{R}^n$ and $u \in \mathbb{R}^m$ the output, the state, and the input of the system, respectively. The matrices $A_1, A_2 \in \mathbb{R}^{n\times n}$, $B \in \mathbb{R}^{n\times m}$, $C \in \mathbb{R}^{p\times n}$, and $H \in \mathbb{R}^n$. The hyperplane defined by $\ker H^T = \{x \in \mathbb{R}^n | H^T x = 0\}$ separates the state space $\mathbb{R}^n$ into two half-spaces. We assume that the vector field of (1) is continuous, which implies that $H^T x = 0$ implies that $A_1 x = A_2 x$. The observer design problem is to synthesize a state estimation procedure, which, on the basis of a known system model, the input u, and the measured output y provides a state estimate $\hat{x}$. In order to do so, we choose the following observer for (1):

$$\dot{\hat{x}} = \begin{cases} A_1 \hat{x} + Bu + L_1(y - \hat{y}), & \text{if } H^T \hat{x} \leq 0 \\ A_2 \hat{x} + Bu + L_2(y - \hat{y}), & \text{if } H^T \hat{x} > 0 \end{cases} \tag{2}$$

with $\hat{y} := C\hat{x}$, $\hat{x} \in \mathbb{R}^n$, and $L_1, L_2 \in \mathbb{R}^{n\times p}$ the output, the observer state, and the observer gain matrices, respectively. As we will show in the following, the observer does not require information on which linear dynamics of the system (1) is currently active as all modes are included in the error dynamics. More specifically, the dynamics of the state estimation error $e = x - \hat{x}$ is described by

$$\dot{e} = \begin{cases} (A_1 - L_1 C)e, & H^T x \leq 0, \quad H^T \hat{x} \leq 0 \\ (A_2 - L_2 C)e + \Delta A x, & H^T x \leq 0, \quad H^T \hat{x} > 0 \\ (A_1 - L_1 C)e - \Delta A x, & H^T x > 0, \quad H^T \hat{x} \leq 0 \\ (A_2 - L_2 C)e, & H^T x > 0, \quad H^T \hat{x} > 0 \end{cases} \tag{3}$$

where $\Delta A := A_1 - A_2$. By substituting $\hat{x} = x - e$ in (3), we see that the right-hand side of the state estimation error dynamics is piece-wise linear in $[e^T \; x^T]^T$. The observer design problem can formally be stated as follows.

Problem: Determine, if possible, observer gains L_1, L_2 in (2) such that global asymptotic stability of the state estimation error dynamics (3) is achieved, for all functions $x(t) : \mathbb{R}^+ \longrightarrow \mathbb{R}^n$, satisfying (1) for some bounded locally integrable input function $u(t) : \mathbb{R}^+ \longrightarrow \mathbb{R}^m$.

Theorem II.1: [12] The state estimation error dynamics (3) is globally asymptotically stable (in the sense of Lyapunov), for all $x(t) : \mathbb{R}^+ \longrightarrow \mathbb{R}^n$ satisfying (1) for a bounded locally integrable input function $u(t) : \mathbb{R}^+ \longrightarrow \mathbb{R}^m$ if there exist matrices $P = P^T > 0$, L_1, L_2, and constants $\lambda_1, \lambda_2 \geq 0$, $\mu > 0$ such that the following set of matrix inequalities is satisfied:

$$\begin{bmatrix} (A_2 - L_2 C)^T P + P(A_2 - L_2 C) + \mu I & P\Delta A + \lambda_1 \frac{1}{2} H H^T \\ \Delta A^T P + \lambda_1 \frac{1}{2} H H^T & -\lambda_1 H H^T \end{bmatrix} \leq 0 \tag{4a}$$

$$\begin{bmatrix} (A_1 - L_1 C)^T P + P(A_1 - L_1 C) + \mu I & -P\Delta A + \lambda_2 \frac{1}{2} H H^T \\ -\Delta A^T P + \lambda_2 \frac{1}{2} H H^T & -\lambda_2 H H^T \end{bmatrix} \leq 0. \tag{4b}$$

Proof: Here we only provide a sketch of the proof. Full details of the proof can be found in [12]. To show that the origin of the observer error dynamics (3) is globally asymptotically stable for all given $x(t) : \mathbb{R}^+ \longrightarrow \mathbb{R}^n$, we prove that $V(e) = e^\top P e$ is a Lyapunov function for (3). To be precise, we use that $P = P^T > 0$ and we will prove that

$$\dot{V} \leq -\mu e^\top e \tag{5}$$

where $\dot{V}$ denotes the right time-derivative of V along solutions of (3). First, we observe that the upper left block of (4a) and (4b) imply that $(A_j - L_j C)^T P + P(A_j - L_j C) < -\mu I$ for $j = 1, 2$.

Hence, for the first and fourth mode of (3) it is clear that (5) holds. To show that (5) also holds for the second and third mode we use the regional information $H^\top x \leq 0$, $H^\top(x-e) > 0$ (second mode), and $H^\top x > 0$, $H^\top(x-e) >\leq 0$ (third mode), which both imply the quadratic constraint

$$\begin{bmatrix} 0 & -\frac{1}{2}HH^\top \\ -\frac{1}{2}HH^\top & HH^\top \end{bmatrix} \leq 0. \tag{6}$$

Hence, if we use this information, we see from (4a) that if $H^\top x \leq 0$, $H^\top(x-e) > 0$, then it holds that

$$\begin{bmatrix} (A_2 - L_2C)^\top P + P(A_2 - L_2C) + \mu I & P\Delta A \\ \Delta A^\top P & 0 \end{bmatrix} \leq 0 \tag{7}$$

and from (4b) we see that if $H^\top x > 0$, $H^\top(x-e) \leq 0$, then it holds that

$$\begin{bmatrix} (A_1 - L_1C)^\top P + P(A_1 - L_1C) + \mu I & -P\Delta A \\ -\Delta A^\top P & 0 \end{bmatrix} \leq 0. \tag{8}$$

This implies that (5) is also satisfied for the second and third mode. This shows that $V(e)$ is a Lyapunov function for (3). Using the usual Lyapunov-based reasoning now completes the proof. ∎

The inequalities (4a) and (4b) are nonlinear matrix inequalities in $\{P, L_1, L_2, \lambda_1, \lambda_2, \mu\}$, but are linear in $\{P, L_1^T P, L_2^T P, \lambda_1, \lambda_2, \mu\}$ and thus can be efficiently solved using linear matrix inequalities solvers, such as LMITOOL for MATLAB [16]. Note that the proposed observer design does not need information about active dynamics nor tries to estimate this explicitly. In case $L_1 = L_2 = L$, the LMI conditions (4) are equivalent to the conditions given in [10]. Conditions for feasibility of the LMI (4) can be formed in [10]. Moreover, the aforementioned theory related to observer design for PWL systems remains conceptually the same for multiple-mode systems. Nevertheless, we will encounter a higher complexity when deriving the observer error dynamics compared to the bimodal case. The reason for that is the fact that there is a quadratic relation between the number of system modes (n) and the number of the modes of the observer error dynamics (n^2). This results in a quadratic increasing number of LMIs, which are numerically more difficult to solve.

B. Observer Design for Lur'e Systems With Multivalued Mappings

Consider the system that is given by the following differential inclusion (see Fig. 1):

$$\dot{x} \in Ax - G\varrho(Hx) + Bu \tag{9}$$

with output $y = Cx$, $A \in \mathbb{R}^{n\times n}$, $B \in \mathbb{R}^{n\times m}$, $H \in \mathbb{R}^{l\times n}$, $C \in \mathbb{R}^{p\times n}$, and $G \in \mathbb{R}^{n\times l}$ has full column rank. We assume that the multivalued mapping ϱ defined on $\mathbb{R}^l$ satisfies the following properties:

- for all $v \in \mathbb{R}^l$ the set $\varrho(v) \subseteq \mathbb{R}^l$ is non-empty, convex, closed, and bounded;
- ϱ is upper semicontinuous (see [17, p. 41]);

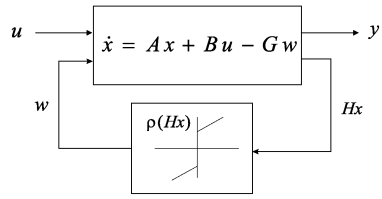

Fig. 1. System with a monotone multivalued mapping in the feedback path.

- ϱ is monotone, i.e., for all $x_1 \in \mathbb{R}^l$ and $x_2 \in \mathbb{R}^l$ it holds that $x_1^* \in \rho(x_1)$ and $x_2^* \in \rho(x_2)$ implies that $\langle x_1^* - x_2^*, x_1 - x_2\rangle \geq 0$, where $\langle\cdot,\cdot\rangle$ denotes the inner product;
- there exist positive constants α and β such that for any $w \in -\varrho(v)$ it holds that $\|w\| \leq \alpha\|v\| + \beta$.

The input functions u are assumed to be in the space of piecewise continuous[1] bounded functions from $[0,\infty)$ to $\mathbb{R}^m$, denoted by PC $(u : [0,\infty) \to \mathbb{R}^m)$. Clearly, the mapping $(t,x) \mapsto Ax - G\varrho(Hx) + Bu(t)$ is upper semicontinuous and attains non-empty, convex, closed, and bounded set-values. From [17, p. 98] or [18, § 7], it follows that local existence of solutions[2] is guaranteed given an initial state x_0 at initial time 0. Due to the growth condition $\|w\| \leq \alpha\|v\| + \beta$, $w \in -\varrho(v)$, it follows that any solution to (9) is globally defined on $[0,\infty)$.

As an observer for the system (9), we propose the following differential inclusion:

$$\dot{\hat{x}} \in (A-LC)\hat{x} - G\varrho\left((H-KC)\hat{x} + Ky\right) + Ly + Bu(t) \tag{10}$$

with output $\hat{y} = C\hat{x}$, $K \in \mathbb{R}^{l\times p}$ and $L \in \mathbb{R}^{n\times p}$. Since the right-hand side is again upper semicontinuous in (t,x) due to continuity of y and piece-wise continuity of u, using the previous properties of ρ it can be shown that global solutions exist of (10). Knowing that both the plant and the observer have global solutions, the observer error dynamics between (9) and (10), with observer error $e := x - \hat{x}$ exists globally and obeys

$$\begin{aligned} \dot{e} &= (A - LC)e - G(w - \hat{w}) \\ w &\in -\varrho(Hx) \\ \hat{w} &\in -\varrho\left(H\hat{x} + K(y - \hat{y})\right). \end{aligned} \tag{11}$$

The problem of the observer design is finding the gains L, K such that all solutions to the observer error dynamics converge exponentially to the origin, which implies that $\lim_{t\to\infty}(\hat{x}(t) - x(t)) = 0$.

The following theorem presents a method for the observer design that requires strict passivity of (A,B,C) which is defined by the existence of a $P = P^\top > 0$ and a $Q = Q^\top > 0$ such that $PA + A^\top P = -Q$ and $B^\top P = C$.

Theorem II.2: Consider the observed system (9), the observer (10), and the observer error dynamics (11). If $(A - LC, G, H - KC)$ is strictly passive, then, the point $e = 0$ is globally

[1]We call a function u piece-wise continuous, if any bounded interval contains at most a finite number of discontinuity points of u.

[2]We call a function $x : [a,b] \to \mathbb{R}^n$ a solution to the differential inclusion $\dot{x}(t) \in F(t, x(t))$, if x is absolutely continuous and satisfies $\dot{x}(t) \in F(t, x(t))$ for almost all $t \in (a,b)$.

exponentially stable. Moreover, the following bound holds:

$$\frac{1}{2}\lambda_{min}(P)e^{\top}(t)e(t) \leq e^{\top}(0)Pe(0)\exp\left(-\frac{\lambda_{min}(Q)}{\lambda_{min}(P)}t\right) \tag{12}$$

where $\lambda_{min}(\cdot)$ denotes the minimal eigenvalue, and matrices P and Q are given by (14).

Proof: Here, we provide a sketch of the proof (for the details see [13]). Note that $e = 0$ is an equilibrium point of (11). Now, let P and Q be positive definite matrices that correspond to the strict passivity conditions $P(A-LC)+(A-LC)^{\top}P = -Q$ and $G^{\top}P = H - KC$ for $(A - LC, G, H - KC)$. To show global exponential stability of the origin of (11), we consider the candidate Lyapunov function $V(e) = (1/2)e^{\top}Pe$. It can be shown that the derivative $\dot{V}$ exists almost everywhere and satisfies (if it exists)

$$\begin{aligned}\dot{V}(e(t)) &= e^{\top}(t)P\dot{e}(t)\\ &= e^{\top}(t)P\left((A-LC)e(t) - G\left(w(t)-\hat{w}(t)\right)\right)\\ &= -\frac{1}{2}e^{\top}(t)Qe(t) - e^{\top}(t)(H-KC)^{\top}\left(w(t)-\hat{w}(t)\right)\end{aligned} \tag{13}$$

for some $w(\cdot), \hat{w}(\cdot)$ satisfying (11). Since

$$\begin{aligned}&e^{\top}(t)(H-KC)^{\top}(w(t)-\hat{w}(t))\\ &\quad = \langle Hx(t) - \{(H-KC)\hat{x}(t) + Ky(t)\}, w(t)-\hat{w}(t)\rangle\end{aligned}$$

with $w(t) \in \varrho(Hx(t))$ and $\hat{w}(t) \in \varrho(H\hat{x}(t) + K(y(t) - \hat{y}(t)))$, it follows from monotonicity of $\varrho(\cdot)$ that $e^{\top}(t)(H - KC)^{\top}(w(t) - \hat{w}(t)) \geq 0$. Therefore, $\dot{V}(e(t)) \leq -(1/2)e^{\top}(t)Qe(t)$ and standard Lyapunov reasoning can be used to derive global exponential stability and the error bound. ■

The gains L and K such that $(A-LC, G, H-KC)$ is strictly passive can be computed by solving the following linear matrix inequalities (see also in [13] and [19]):

$$\begin{aligned}&P = P^{T} > 0\\ &(A-LC)^{\top}P + P(A-LC) + \nu I < 0\\ &G^{\top}P = H - KC\end{aligned} \tag{14}$$

where $\nu > 0$. For a given ν, inequality (14) is a linear matrix inequality in P, K, and $L^{\top}P$. According to (12), the rate of convergence depends on the eigenvalues of the matrix Q and P, which in turn depend on the system parameters. When solving the LMIs for observer design the size of both matrices can be "controlled," for example, by tuning ν or by adding the constraint $P < \gamma I$ and my including scalar variables (such as γ and ν) in the optimization objective. The computed output feedback gains will then guarantee the rate of convergence as in (12). Note that this tuning is allowed since the provided LMI is a conservative constraint. The conservatism of this constraint is due to the fact that it is based on a Lyapuvov-based approach. For details on numerical schemes for computing the solutions to observer dynamics (10), we refer the reader to [13] and [19].

III. Observer Design Implementation on a PWL Beam System

In this brief, we implement the observer discussed in Section II-A to a PWL beam system [a harmonically excited flexible beam supported by a one-sided spring, see Fig. 2(a)] and we show, based on simulation and experimental results, that the non-smooth observer reconstructs with high accuracy the dynamics of the examined system.

A. Experimental PWL Beam Setup

The experimental setup as shown in Fig. 2(a) consists of a steel beam supported at both ends by two leaf springs. A second beam, clamped at both ends, is located parallel to the first one and acts as a one-sided spring. This one-sided spring represents a non-smooth nonlinearity in the dynamics of the beam system. In case the spring is linear and the impact between the one-sided spring and the beam is negligible, the beam system can be described as a PWL system. The beam is excited by a force u generated by a rotating mass-unbalance, which is mounted at the middle of the beam. A tacho-controlled motor, that enables a constant rotational speed, drives the mass-unbalance. In the experimental setup, the displacements at two positions can be measured using linear voltage displacement transducers (with a sensor accuracy in the order of 10^{-6} m). For further information on the experimental setup, the reader is referred to [20] and [21]. When the beam moves from its rest point towards the one-sided spring, the spring is active. Therefore, the system has different dynamics on this side than on the opposite side. In the first case, the system dynamics is determined by the stiffness of the beam and the spring, in the second case, only by the beam stiffness. The switching boundary between the two dynamic regimes is present at zero displacement of the middle of the beam.

In order to describe the behavior of the beam accurately, a 111 degrees-of-freedom (DOF) finite-element model (FEM) has been developed (see [22]). Due to the large number of model DOFs, the simulation of the nonlinear responses is computationally expensive. In order to decrease the computational time we develop a reduced model, which is based on the FEM, by using a dynamic component mode synthesis reduction method, the so-called Rubin method [23]. The reduced model has three degrees-of-freedom, see [22], [24], and is described by

$$M_r\ddot{q} + B_r\dot{q} + K_r q + f_{nl}(q) = hu(t) \tag{15}$$

where $h = [1\ 0\ 0]^T$ and $q = [q_{\text{mid}}\ q_{\text{act}}\ q_{\xi}]^T$. Herein, q_{mid} is the displacement of the middle of the beam and q_{act} is the displacement of the point depicted in Fig. 2(b). Moreover, q_{ξ} reflects the contribution of the first eigenmode of the beam and M_r, B_r, and K_r are the mass, damping, and stiffness matrices of the reduced model, respectively. We apply a periodic excitation force $u(t) = u_0 \sin\omega t$, which is generated by the rotating mass-unbalance at the middle of the beam. Moreover, the restoring force of the one-sided spring is $f_{nl}(q) = k_{nl}\, h\, \min(0, h^T q) = k_{nl}\, h\, \min(0, q_{\text{mid}})$, where k_{nl} is the stiffness of the one-sided

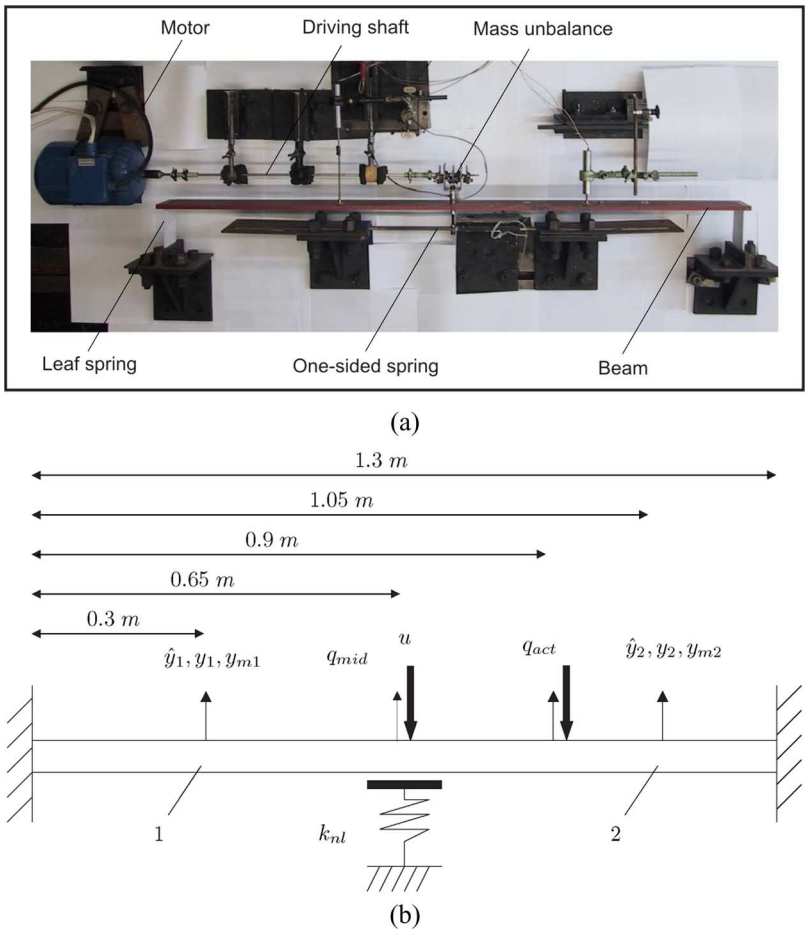

Fig. 2. (a) Photo of the experimental PWL beam setup system. (b) Scheme of the experimental PWL beam setup.

spring. Model (15) can be written in the form (1), where $x = [q^T \ \dot{q}^T]^T$, $H = [h^T \ 0_{3\times 1}^T]^T$

$$A_1 = \begin{bmatrix} 0_{3\times 3} & I_{3\times 3} \\ -M_r^{-1}(K_r + k_{nl}hh^T) & -M_r^{-1}B_r \end{bmatrix}$$
$$A_2 = \begin{bmatrix} 0_{3\times 3} & I_{3\times 3} \\ -M_r^{-1}K_r & -M_r^{-1}B_r \end{bmatrix}$$
$$B = \begin{bmatrix} 0 \\ M_r^{-1}h \end{bmatrix}.$$

Herein, $k_{nl} = 198\,000$ (N/m), while the numerical values of M_r[kg], K_r[N/m], B_r[Ns/m] are

$$M_r = \begin{bmatrix} 4.494 & -2.326 & 0.871 \\ -2.326 & 7.618 & 2.229 \\ 0.871 & 2.229 & 2.374 \end{bmatrix}$$
$$K_r = 10^6 \begin{bmatrix} 2.528 & -0.345 & 1.026 \\ -0.345 & 1.051 & 0.296 \\ 1.026 & 0.296 & 0.613 \end{bmatrix}$$
$$B_r = 10^2 \begin{bmatrix} 1.173 & -0.298 & 0.416 \\ -0.298 & 1.041 & 0.314 \\ 0.416 & 0.314 & 0.365 \end{bmatrix}.$$

The output y of the model will be the displacement y_1 [see Fig. 2(b)]. Note that the LMIs in (4) must be feasible for this output.

B. Observer Design, Simulation, and Experimental Results for the PWL Beam Setup

For the complete state reconstruction of the beam system only a transversal displacement y_1 of a single point on the beam is needed [point 1 in Fig. 2(b)]. Nevertheless, the displacement y_2 of a second point [point 2 in Fig. 2(b)] is also measured in order to experimentally validate the obtained results.

This means, $y_1 = C_1 x$ is output of the plant and $y_2 = C_2 x$ is used for validation purposes, with $C_1 = [-0.9579\ 1.2165\ -0.2642\ 0\ 0\ 0]$ and $C_2 = [0.0801\ -1.2013\ -0.8669\ 0\ 0\ 0]$ (see [15]). Using y_1 for observer output injection, the observer reconstructs the full state $(\hat{x})$, and consequently, the displacement $(\hat{y}_2 = C_2\hat{x})$ of the second point on the beam.

By solving the LMIs (4a) and (4b) the observer gains L_1 and L_2 are calculated. The numerical values of these gains are $L_1 = 10^5 \cdot [0.134\ 0.145\ -0.353\ 5.402\ 9.448\ -26.46]$, $L_2 = 10^5 \cdot [0.134\ 0.145\ -0.353\ 7.99\ 10.893\ -28.705]$. A detailed description for the L_1 and L_2 computation is given in Section V. In Figs. 3(a.1), (b.1), and (b.2), y_2 is compared with $\hat{y}_2$ for different excitation frequencies ω and different excitation amplitudes u_0 of the harmonic excitation u in simulations. Furthermore, the estimation error $e_o = \hat{y}_2 - y_2$ is depicted in Fig. 3(a.2). In this figure, it is shown that the estimation error converges to zero, as guaranteed by the theory. The estimation error settling time is less than 0.7 s. In Fig. 3(c) and (d), the model and observer estimations of the displacement of the

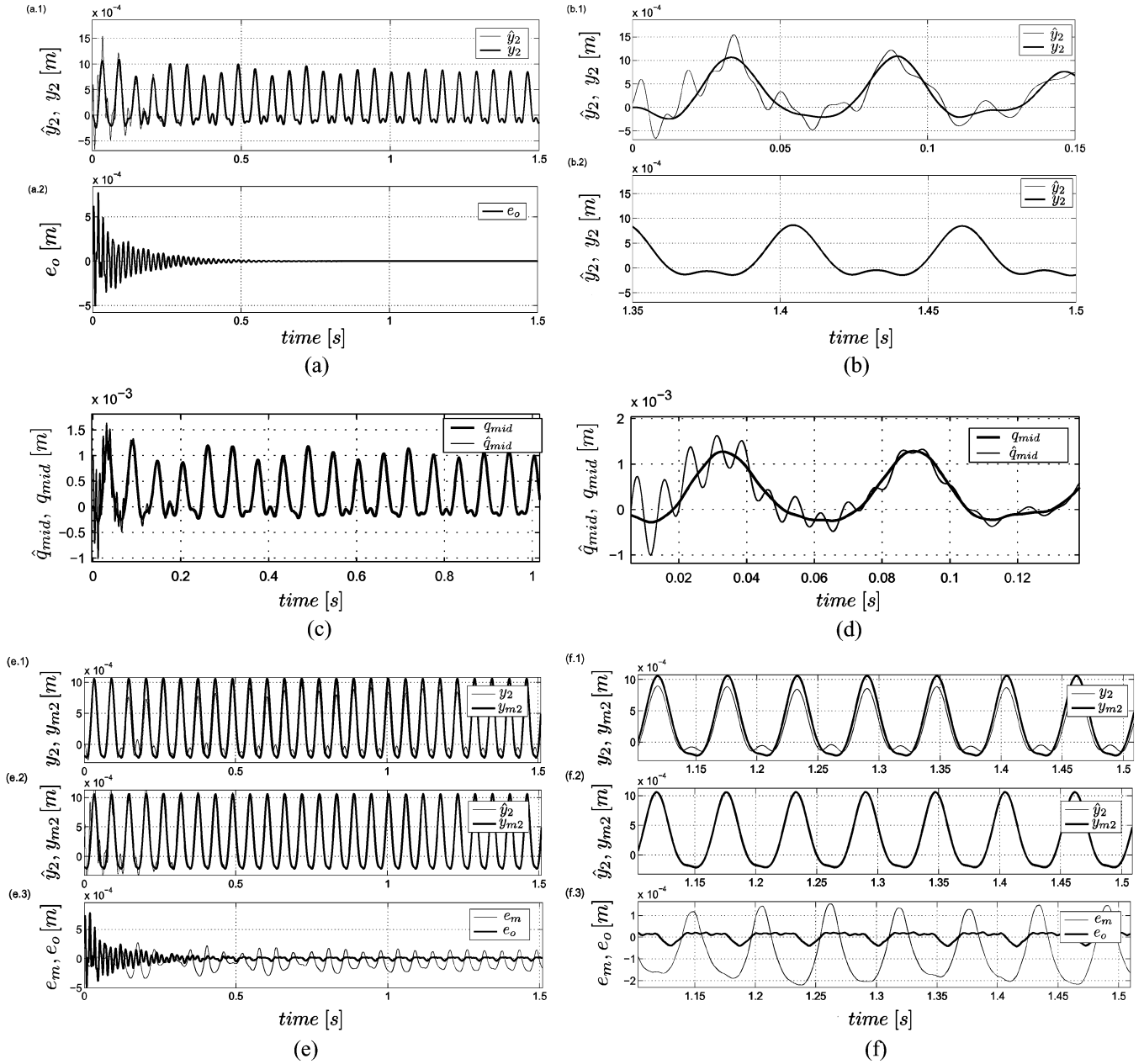

Fig. 3. (a.1) Model prediction y_2 [m] and observer reconstruction $\hat{y}_2$ [m]. (a.2) Estimation error e_o [m]. (b.1) Zoomed version of (a.1) in the transient state. (b.2) Zoomed version of (a.1) in steady-state. (c) Model prediction $q_{\rm mid}$ [m] and observer reconstruction $\hat{q}_{\rm mid}$ [m]. (d) Zoomed version of (c) in the transient state. (e.1) Measured displacement y_{m2} [m] and model prediction y_2 [m]. (e.2) Measured displacement y_{m2} [m] and observer reconstruction $\hat{y}_2$ [m]. (e.3) Estimation error e_o [m] and model error e_m [m]. (f.1) Zoomed version of (e.1). (f.2) Zoomed version of (e.2). (f.3) Zoomed version of (e.3). The excitation frequency is $\omega/2\pi = 35$ Hz and the excitation amplitude is $u_0 = 50$ N.

middle of the beam are depicted. In Fig. 3(d), we show that the model and the observer do not switch dynamics simultaneously. Nevertheless, both converge to the same steady-state solution, as can be seen in Fig. 3(c). The initial conditions for the model and the observer are $x_0 = [0\,0\,0\,0\,0\,0]^T$, $\hat{x}_0 = [10^{-3}\,0\,0\,0\,0\,0]^T$.

In order to examine experimentally whether the observer reconstructs the real state of the system, a comparison between the measured displacement (y_{m2}) of a point along the beam [point 2 in Fig. 2(b)] with the corresponding model prediction and observer estimation (y_2, $\hat{y}_2$) is performed. The output injection used here is the measured displacement (y_{m1}) of the point 1 in Fig. 2(b). In Fig. 3(e.1), (e.2), (f.1), and (f.2), y_2 and $\hat{y}_2$ are compared with y_{m2}. Furthermore, the estimation error $e_o = \hat{y}_2 - y_{m2}$ and the model error $e_m = y_2 - y_{m2}$ are depicted in Fig. 3(e.3) and (f.3). The initial conditions x_0, $\hat{x}_0$ are the same as in simulations.

Clearly, the observer accurately reconstructs y_2. Furthermore, a difference between y_{m2} and y_2 exists [e.g., see Fig. 3(f.1)] due to an (inevitable) model mismatch and due to noise in the measured signals. Since the observer is based on a model including such inevitable mismatch and since it uses as output injection a signal contaminated by noise we expect that e_o will also be affected by these inaccuracies. Nevertheless, e_o is considerably smaller than e_m in all results (at least a factor of three

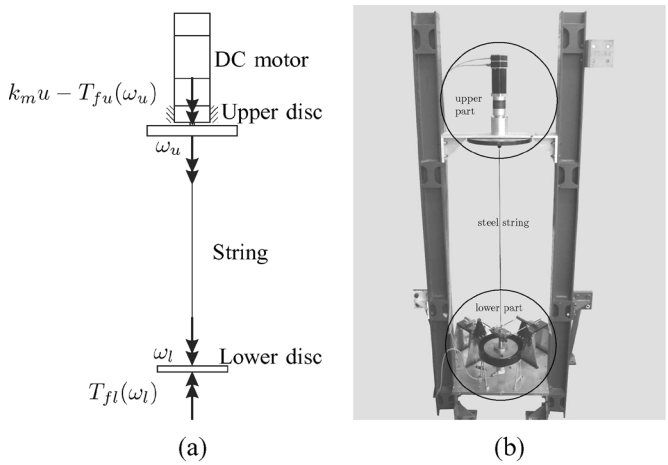

Fig. 4. (a) Scheme of the experimental dynamic rotor system. (b) Photo of the experimental dynamic rotor system.

smaller). Moreover, it is worth mentioning that e_o converges to its steady-state solution faster than e_m. Providing somewhat more numerical details, in Fig. 3(e.3) e_o and e_m converge to their steady-state response within 0.5 and 0.7 s, respectively. The maximum absolute value of the amplitude of e_o and e_m in steady-state is 2×10^{-5} m and 2.2×10^{-4}m, respectively.

The mismatch between the model and the experimental PWL beam is caused by series of factors. For instance, the model assumes that the one-sided spring is massless while in reality it is not. This means that, in the model, the contact between the beam and the spring occurs very smoothly, while in reality there is an impact between the beam and the spring every time the middle of the beam touches the one-sided spring. Furthermore, the model contains only the dynamic modes in the frequency band $[0 < \omega/(2\pi) \leq 60]$ Hz, while we compensate for the remaining modes, see [23]. For an online implementation of the observer design strategy, the observer should be based on a simple model in order to ensure fast online state reconstruction.

IV. Observer Design Implementation on a Dynamic Rotor System

In this brief, we present the experimental implementation of the observer proposed in Section II-B to a dynamic rotor system [two inertias, coupled by a flexibility, of which one is subject to friction and the other is driven by an actuator, see also Fig. 4(b)]. Moreover, using simulation and experimental results, we show that the observer can accurately predict the dynamical behavior of this system.

A. Experimental Setup for a Dynamic Rotor System

The experimental setup is shown in Fig. 4(a) and (b). The input voltage from the computer, which is between -5 and 5 V, is fed into the dc-motor via the power amplifier. The dc-motor is connected to the upper steel disc, via the gear box. The upper and lower discs are connected through a low-stiffness steel string. Both discs can rotate around their geometric centers and the related angular positions are measured using incremental encoders. Moreover, an additional brake is applied at the lower disc and creates a friction that induces limit cycling to the system.

In order to derive a simple, though predictive, model for the dynamic rotor system we assume that the dc motor dynamics does not influence the system's dynamics, the lower disc remains always horizontal and it does not move in vertical and lateral direction, the torsional damping in the string is negligible with respect to the damping of the bearings of the discs and the string is massless (for more details see [25]).

The experimental dynamic rotor system can be described by the following model:

$$\begin{aligned} J_u\ddot{\theta}_u + k_\theta(\theta_u - \theta_l) + T_{fu}(\dot{\theta}_u) &= k_m u \\ J_l\ddot{\theta}_l - k_\theta(\theta_u - \theta_l) + T_{fl}(\dot{\theta}_l) &= 0 \end{aligned} \tag{16}$$

where θ_u and θ_l are the angular positions of the upper and lower discs, respectively. Moreover, u is the input voltage to the power amplifier of the motor, J_u and J_l are the moments of inertia of the upper and lower discs about their respective centers of mass, k_θ is the torsional spring stiffness, and k_m is the motor constant. The friction torques T_{fu} and T_{fl} act on the upper and lower disc, respectively. The friction torque at the upper disc $T_{fu}(\dot{\theta}_u)$ is caused by friction in the bearings of the upper disc and the electro-magnetic effect in the dc-motor. The friction torque at the lower disc $T_{fl}(\dot{\theta}_l)$ comprises the friction in the bearings of the lower disc and the friction induced by the brake mechanism.

The dynamics of the system (16) can be described by a third-order state-space system since its dynamics only depends on the difference between the two angular positions and their velocities. Therefore, by choosing the state variables as $x_1 = \theta_u - \theta_l$, $x_2 = \dot{\theta}_u$, and $x_3 = \dot{\theta}_l$, the following state-space model can be obtained

$$\begin{aligned} \dot{x}_1 &= x_2 - x_3 \\ \dot{x}_2 &= \frac{k_m}{J_u}u - \frac{k_\theta}{J_u}x_1 - \frac{1}{J_u}T_{fu}(x_2) \\ \dot{x}_3 &= \frac{k_\theta}{J_l}x_1 - \frac{1}{J_l}T_{fl}(x_3). \end{aligned} \tag{17}$$

The parameters k_m, J_u, J_l, k_θ, and the models of T_{fu} and T_{fl} are identified experimentally in [25] and [26]. In [25] and [26], it is indicated that the viscous friction due to the electro-magnetic effect in the motor dominates the friction $T_{fu}(x_2)$ at the upper disc. Therefore, we can take that $T_{fu}(x_2) = b_{up}x_2$. Furthermore, the friction at the lower disc can be modeled accurately with a set-valued dry friction model with negative damping (Stribeck effect [27], [28]), shown in (18) at the bottom of the page, where T_{sl}, T_1, T_2, w_1, w_2, and b_l are the parameters of the friction model. Moreover, $-T_{sl}$ and T_{sl} represent the minimum and the maximum static friction level, respectively, and b_l is the viscous friction coefficient. The

$$T_{fl}(x_3) \in \begin{cases} \left(T_{sl} + T_1\left(1 - \frac{2}{1+e^{w_1|x_3|}}\right) + T_2\left(1 - \frac{2}{1+e^{w_2|x_3|}}\right)\right)\operatorname{sign}(x_3) + b_l x_3, & \text{for } x_3 \neq 0 \\ [-T_{sl}, T_{sl}], & \text{for } x_3 = 0 \end{cases} \tag{18}$$

TABLE I
PARAMETER VALUES OF THE MODEL (17), (18)

Parameter	Estimated value
J_u [kg m^2/rad]	0.4765
k_m [Nm/V]	3.9950
b_{up} [Nms/rad]	2.2247
k_θ [Nm/rad]	0.0727
J_l [kgm^2/rad]	0.0326
T_{sl} [Nm]	0.1642
T_1 [Nm]	0.0603
T_2 [Nm]	-0.2267
w_1 [s/rad]	5.7468
w_2 [s/rad]	0.2941
b_l [Nms/rad]	0.0109

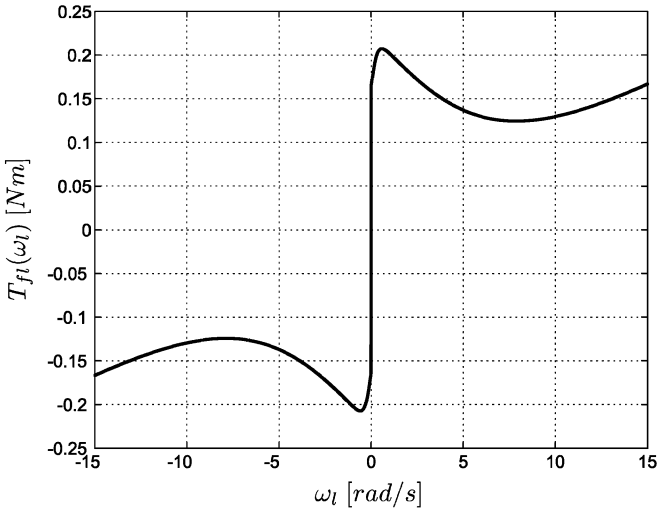

Fig. 5. Dry friction model $T_{fl}(\omega_l)$ at the lower disc.

identified parameters of the model (17) and (18) are given in Table I. The friction law (18) with the parameters from Table I is depicted in Fig. 5.

The mapping which describes the friction force at the lower disc is not monotone (see Fig. 5) but can be transformed into a monotone mapping using the technique of loop transformation [29]. The new friction mapping is defined as $\tilde{T}_{fl}(\omega) = T_{fl}(\omega) - m\omega$, where $m = -0.02$ is the maximal negative slope of the graph in Fig. 5. The system matrix A is replaced by $\tilde{A} = A - mGH$. The model of the setup now takes the form

$$\dot{x} \in \tilde{A}x + Bu - G\tilde{T}_{fl}(Hx) \quad y = Cx \tag{19}$$

which is in the form of (9) with $H = [0\ 0\ 1]$, $C = [1\ 0\ 0]$, $B = [0\ 8.3841\ 0]$, $G = [0\ 0\ 30.6748]$

$$A = \begin{bmatrix} 0 & 1.00 & -1.00 \\ -0.1526 & -4.6688 & 0 \\ 2.2301 & 0 & 0 \end{bmatrix}.$$

It should be noted that although the friction model is rather simple (static), it accurately describes the discontinuous dynamics of the system (see [26]). Furthermore, system (19) satisfies the conditions proposed in Section II-B.

B. Observer Design, Simulation, and Experimental Results for the Experimental Dynamic Rotor System

For the complete state reconstruction of the dynamic rotor system, the difference between the measured angular positions of the two discs is used as an output injection signal, i.e., $y = x_1$. For the validation of the observer for the dynamic rotor system we, first, show that the observer can reconstruct the state of the model and, second, we experimentally show that it can reconstruct the output (thus the state) of the real system.

For the observer design, we will use $y = x_1$ as a measured output, which is the difference between the angular positions of the two discs. These angular positions are measured using incremental encoders. The observer will provide estimates for the other state variables (i.e., also the velocities of upper and lower discs). In simulations and experiments we will compare the estimated values of the state variables with the measured values. Due to the fact that velocities are not measured, in order to provide a comparison measure for the estimated velocities based on the observer (10), we also derive the velocities of the discs by numerically differentiating the angular positions of the discs and filtering the resulting signals using a low-pass filter. The high resolution of the encoders ($\approx 10^{-3}$ rad) allows for accurate computation of the aforementioned velocities.

The observer design of the form (10) for system (19), entails finding gains L and K such that the triple $(\tilde{A}-LC, G, H-KC)$ is strictly passive. By solving LMIs (14) using the LMITOOL for MATLAB [16] we found that $L = [2.476\ 5.199\ -26.220]$ and $K = -2.025$ satisfy (14). For simulation purposes, the input signal u in (17) is chosen to be a constant signal $u = 2$ V. The case of constant inputs is considered, since in this dynamic rotor system the steady-state behavior to constant inputs is of great interest; equilibria, represented by constant velocities, are considered desirable, whereas stick-slip limit-cycling is considered to be an unwanted vibrational phenomenon. At this point, we present simulations for the initial state for the system taken as $x(0) = [0\ 0\ 0]^\top$ and for the observer as $\hat{x}(0) = [3\ 3\ 3]^\top$. The solution of (17) is constructed using a dedicated technique for simulating systems with set-valued friction based on the switched friction model presented in [30] while the observer is simulated using numerical schemes presented in [13] and [19].

The simulation results are depicted in Fig. 6(a) and the (squared) estimation error $(e^T e)$ is depicted in Fig. 6(c). When a constant input voltage is applied (i.e., a constant torque is applied to the upper disc) stick-slip oscillations (torsional vibrations) occur due to the negative damping in the friction law (18). During these oscillations, the velocity x_3 of the lower disc alternates between zero (stick phase) and positive values (slip phase). As guaranteed by the theory, the designed observer is able to provide the correct estimate of the state. Moreover, based on (12), we can provide a bound on the decrease of the squared estimation error. This bound is indicated by the dashed line in Fig. 6(c). From Fig. 6(c), we can conclude that the squared estimation error $(e^T e)$ does not converge to zero exactly, but a small residual value $(\approx 10^{-3})$ remains after 3.7 s. When simulating the differential inclusions (10) and (17) there are two sources of numerical errors. The first is due to the time discretization introduced by the numerical method itself. The

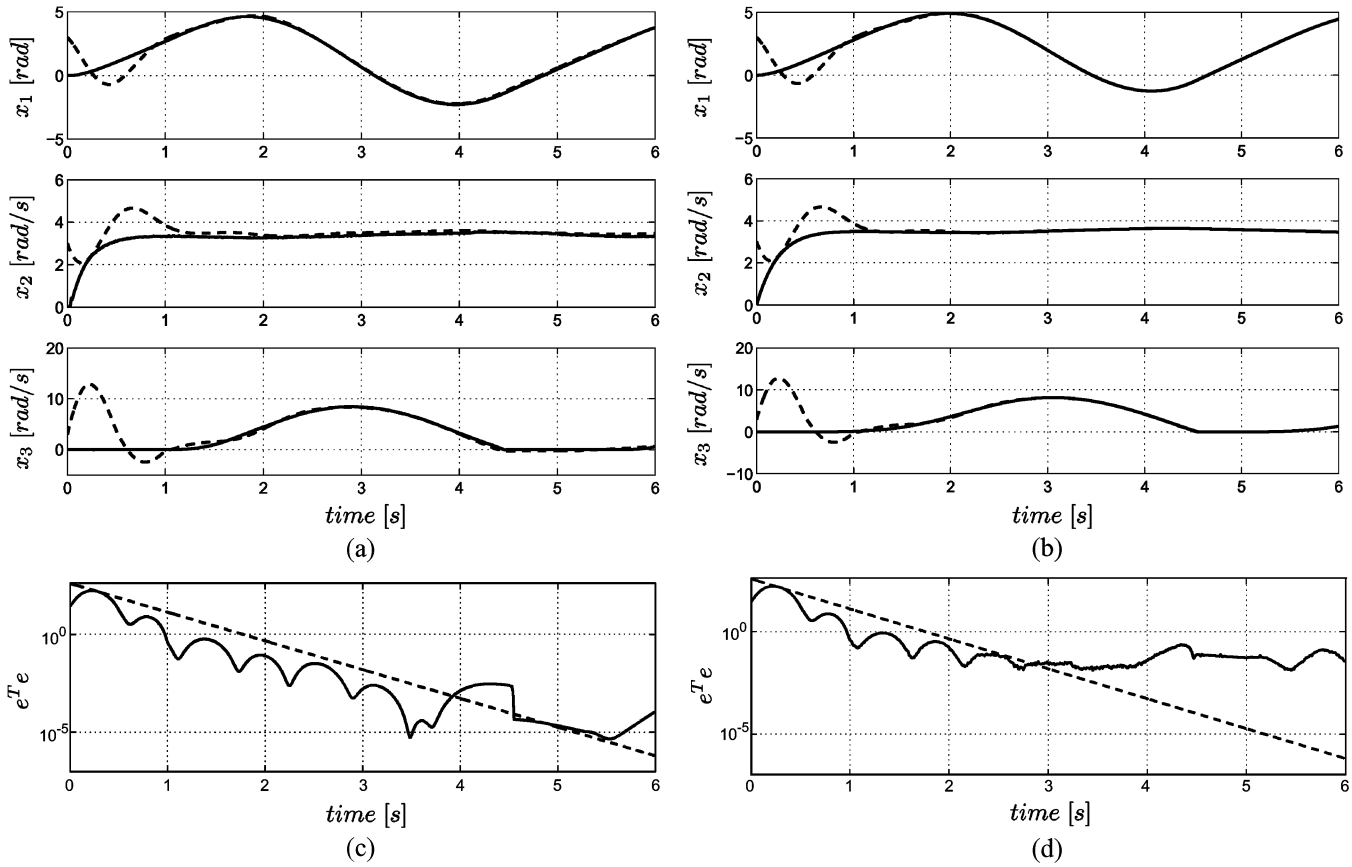

Fig. 6. (a) Simulated responses of the system (solid line) and the observer (dashed line): x_1 (upper), x_2 (middle), x_3 (lower) under the constant input voltage $u = 2$ V. (b) Measured and computed responses x_1, x_2, x_3 (solid line), and the observer estimates $\hat{x}_1$, $\hat{x}_2$, $\hat{x}_3$ (dashed line): x_1 (upper), x_2 (middle), x_3 (lower) under the constant input voltage $u = 2$ V. (c) The norm of the simulated estimation error (solid line) and the theoretical bound of the error norm (dashed line), on a logarithmic scale. (d) The norm of the experimental estimation error (solid line) and the theoretical bound of the error norm (12) (dashed line), on a logarithmic scale.

second source of numerical errors stems from the fact that at each time step a system of nonlinear equations has to be solved and the used solvers have finite precision.

As it was mentioned in the beginning of Section IV-B, the response x_1 of the experimental setup is measured and the responses x_2, x_3 are computed (using numerical differentiation of the measured displacements of the upper and lower discs) under the same input voltage ($u = 2$ V) as for the simulations. The measured state component x_1, the computed state components (x_2, x_3) and the estimate state components ($\hat{x}_1$, $\hat{x}_2$, $\hat{x}_3$) are depicted in Fig. 6(b). The experimental squared error $e^T e$ is depicted together with the theoretical bound (12) in Fig. 6(d).

The experimental results show that the designed observer is able to provide accurate estimates of the state of the experimental setup. The squared estimation error $e^T e$ does not converge to zero exactly, but oscillates around the value of approximately 10^{-1} rad^2 after 3.7 s. This error is small compared to the magnitude of the state, but larger than in the simulation results. The residual error can be attributed to (inevitable) model errors and sensor imperfections.

V. Discussion

The mismatch between the observer and the experimental PWL beam or the dynamic rotor system [see the remaining estimation error e_o in Figs. 3(f.3) and 6(d)] is the guide line for the evaluation of the computed observer gains (L_1, L_2) or (L, K), in terms of fast transient convergence and low sensitivity to model errors and measurement noise. More specifically, we compute different observer gains that satisfy the LMI constraints (4) (for the beam system) or the LMI constraints (14) (for the dynamic rotor system) by varying the constants μ and ν, respectively. For every pair of observer gains (L_1, L_2) or (L, K) we can measure the magnitude of e_o or $e_o^T e_o$ (for the PWL beam or the dynamic rotor system, respectively) in steady-state and the time (settling time) required for e_o to converge to its steady-state. By increasing, for example, μ or ν we guarantee a faster settling time. Nevertheless, this results in higher observer gains and, as a consequence, in an increase in the system's noise sensitivity.

The knowledge of e_o or $e_o^T e_o$ can then be used to assess the effect of the choice of the observer gain on both the transient performance and the steady-state sensitivity to modelling errors and measurement noise. This is exactly the trade off between such transient and steady-state performance that determines the ultimate choice for the observer gains. Clearly, the desired balance between transient and steady-state performance heavily depends on the specific performance requirements for the system under study. The specific observer gains used in this brief are obtained by balancing such transient and steady-state performance for the PWL beam system and the dynamic rotor system with friction.

In order to further reduce the model errors and the measurement noise in the examined benchmark setups aiming at even higher steady-state performance, we could use more accurate (more complex) models to describe the system dynamics. Furthermore, high precision encoders are needed in order to decrease the measurement noise in the signals that are used to recover the system state. The drawback of aiming at more accurate models is that, in most of the cases, it will lead to models of higher order and/or higher complexity. As a result, the calculation of the observer responses becomes (too) computationally expensive. This is not favorable for the online implementation of observer designs in real systems. Moreover, the drawback of using high precision encoders is that they are generally expensive.

VI. Conclusion

In this brief, we have presented observer designs and experimental implementations for two types of systems; non-smooth continuous systems and discontinuous systems. More specifically, we designed and applied a PWL observer for a periodically excited beam with one-sided flexible support and a discontinuous observer for an experimental dynamic rotor system with discontinuous friction. Generally speaking, to show the strengths, weaknesses, and potential of any observer design beyond their theoretical importance, it is indispensable to evaluate them in experimental and industrial setups. The presented case studies can be considered as benchmarks for observer design for non-smooth and discontinuous systems as they are prototypical for entire classes of engineering systems. The beam system is representative for mechanical systems with one-sided restoring characteristics and the rotor dynamic system is representative for motion systems with friction.

The assessment of the performance of the implemented observers is based on both simulation and experimental results. According to these results the observers perform well, since they predict with high accuracy the real system responses, despite the presence of unavoidable modeling inaccuracies and measurement noise. These results are promising as we used relatively simple low-order models, which, however, exhibit non-smooth or discontinuous characteristics. Such models are shown to be highly predictive for the examined experimental systems while having limited model complexity. This motivates, first, the validity of non-smooth, discontinuous modelling for engineering systems and, second, the need for the design of model-based observers for non-smooth, discontinuous systems, as shown in this brief.

The current line of work will be continued by the design of output-feedback controllers for the considered classes of systems based on the implemented observers and the application of such controllers to the experimental setups.

References

[1] S. Doole and S. Hogan, "A piecewise linear suspension bridge model: Nonlinear dynamics and orbit continuation," *Dyn. Stability Syst.*, vol. 11(1), pp. 19–47, 1996.

[2] D. van Campen, R. Fey, F. van Liempt, and A. de Kraker, "Steady-state behaviour of a solar array system with elastic stops," in *Proc. IUTAM Symp. New Appl. Nonlinear Chaotic Dyn. Mechan.*, 1998, pp. 303–312.

[3] J. Thompson and H. Stewart, *Nonlinear Dynamics and Chaos; Geometrical Methods for Engineers and Scientists*. New York: Wiley, 1986.

[4] N. Mihajlović, N. van de Wouw, M. Hendriks, and H. Nijmeijer, "Friction-induced limit cycling in flexible rotor systems: An experimental drill-string set-up," *Nonlinear Dyn.*, vol. 46, no. 3, pp. 273–291, 2006.

[5] A. Juloski, W. Heemels, and G. Ferrari-Trecate, "Data-based hybrid modelling of the component placement process in pick-and-place machines," *Control Eng. Practice*, vol. 12, no. 10, pp. 1241–1252, 2004.

[6] F. Pfeiffer and M. Hajek, "Stick-slip motions in turbine blade dampers," *Philosophical Trans. Royal Soc. London*, vol. 338, pp. 503–517, 1992.

[7] J. J. Slotine, J. K. Hedrick, and E. A. Misawa, "On sliding observers for nonlinear systems," *ASME Dynam. Syst. Meas.*, vol. 109, pp. 245–252, 1987.

[8] E. van de Vorst, D. van Campen, R. Fey, A. de Kraker, and J. Kok, "Vibration control of periodically excited nonlinear dynamic multi-DOF systems," *J. Vibr. Control*, vol. 1, pp. 75–92, 1995.

[9] C. Cruz, H. Nijmeijer, and A. Aguilar, "Synchronization of a noisy Chua circuit via two switching Kalman filters," *J. Mexican Soc. Instrumentation*, vol. 5, no. 3, pp. 162–169, 2002.

[10] M. Arcak and P. Kokotović, "Observer based control of systems with slope-restricted nonlinearities," *IEEE Trans. Autom. Control*, vol. 46, no. 7, pp. 1146–1150, Jul. 2001.

[11] X. Fan and M. Arcak, "Observer design for systems with multi-variable monotone nonlinearities," *Syst. Control Lett.*, vol. 50, pp. 319–330, 2003.

[12] A. Juloski, W. Heemels, and S. Weiland, "Observer design for a class of piece-wise linear systems," *Int. J. Robust Nonlinear Control*, vol. 17, no. 15, pp. 1387–1404, 2007.

[13] W. Heemels, A. Juloski, and B. Brogliato, "Observer and control design for Lure's systems with multivalued mappings," presented at the 16th IFAC World Congr., Prague, Czech Republic, 2005.

[14] B. Brogliato, "Absolute stability and the Lagrange-Dirichlet theorem with monotone multivalued mappings," *Syst. Control Lett.*, vol. 51, pp. 343–353, 2004.

[15] A. Doris, A. Juloski, M. Heemels, N. v. d. Wouw, and H. Nijmeijer, "Switching observer design for an experimental piece-wise linear beam system," presented at the 16th IFAC Conf., Prague, Czech Republic, 2005.

[16] L. El Ghaoui and J. Commeau, "LMITOOL: A package for LMI optimization in Scilab user's guide," 1999 [Online]. Available: http://robotics.eecs.berkeley.edu/elghaoui/lmitool/lmitool.html

[17] J.-P. Aubin and A. Cellina, *Differential Inclusions*. Berlin, Germany: Springer-Verlag, 1984.

[18] A. F. Filippov, *Differential Equations With Discontinuous Righthand Sides*, ser. Mathematics and Its Applications. Dordrecht, The Netherlands: Kluwer, 1988.

[19] A. Juloski, "Observer design and identification methods for hybrid systems: Theory and experiments," Ph.D. dissertation, Dept. Elect. Eng., Eindhoven Univ. Technol., Eindhoven, The Netherlands, 2004.

[20] E. van der Vorst, "Long term dynamics and stabilization of nonlinear mechanical systems," Ph.D. dissertation, Dept. Mechan. Eng., Eindhoven Univ. Technol., Eindhoven, The Netherlands, 1996.

[21] M. Heertjes, "Controlled stabilization of long-term solutions in a piecewise linear beam system," Ph.D. dissertation, Dept. Mechan. Eng., Eindhoven Univ. Technol., Eindhoven, The Netherlands, 1999.

[22] J. Bonsel, R. Fey, and H. Nijmeijer, "Application of a dynamic vibration absorber to a piecewise linear beam system," *Nonlinear Dyn.*, vol. 37(3), pp. 227–243, 2004.

[23] R. Craig, "A review of time-domain and frequency-domain component mode synthesis methodes, combined experimental/analytical modeling of dynamic structural systems using substructure synthesis," *ASME Appl. Mechanics*, vol. 67, pp. 1–31, 1985.

[24] R. Fey, "Steady-state behaviour of reduced dynamics with local nonlinearities," Ph.D. dissertation, Dept. Mechan. Eng., Eindhoven Univ. Technol., Eindhoven, The Netherlands, 1992.

[25] N. Mihajlović, A. A. van Veggel, N. v. d. Wouw, and H. Nijmeijer, "Analysis of friction-induced limit sysling in an experimental drill-string system," *ASME J. Dyn. Syst., Meas. Control*, vol. 126, no. 4, pp. 709–720, 2005.

[26] N. Mihajlović, "Torsional and lateral vibrations in flexible rotor systems with friction," Ph.D. dissertation, Dept. Mechan. Eng., Eindhoven Univ. Technol., Eindhoven, The Netherlands, 2005.

[27] B. Armstrong-Hélouvry, P. Dupont, and C. Canudas de Wit, "Survey of models, analysis tools and compensation methods for the control of machines with friction," *Automatica*, vol. 30, no. 7, pp. 1083–1138, 1994.

[28] C. Canudas de Wit, P. Noel, A. Aubin, and B. Brogliato, "Adaptive friction compensation in robot manipulators: Low-velocities," *Int. J. Robot. Res.*, vol. 10, no. 3, pp. 189–199, 1991.

[29] M. Vidyasagar, *Nonlinear Systems Analysis*. Englewood Cliffs, NJ: Prentice-Hall, 1993.

[30] R. I. Leine, D. H. van Campen, A. de Kraker, and L. van den Steen, "Stick-slip vibrations induced by alternate friction models," *Nonlinear Dyn.*, vol. 16, pp. 41–54, 1998.